Complex dynamics and quantum tunneling in the presence of chaos(New Trends and Applications of Complex Asymptotic Analysis : around dynamical systems, summability, continued fractions)

AUTHOR(S):

Shudo, Akira

数理解析研究所講究録
1493巻 2006年 118-134

Complex dynamics and quantum tunneling in the presence of chaos

Akira Shudo
首藤 啓 (首都大学東京 物理)

Department of Physics, Tokyo Metropolitan University,
1-1 Minami-Ohsawa, Hachioji, Tokyo 192-0397, Japan
shudo@phys.metro-u.ac.jp

1 Introduction

Tunneling phenomenon is peculiar to quantum mechanics and no counterparts exist in classical mechanics. Features of tunneling are nevertheless strongly influenced by underlying classical dynamics [1, 2, 3, 4, 5]. One of the most efficient methods to analyze quantum tunneling processes is the WKB or semiclassical method in which the classical orbits are employed as inputs of approximation. However, since quantum tunneling is an essentially classically forbidden process, *real* classical orbits have no ability to describe it, instead the complex classical orbits play central roles.

It should be recalled that using complex orbits itself is not new in the WKB theory, rather it goes back to the beginning of the WKB theory, especially a text book example of quantum tunneling in one dimension. Also, a well-known technique using the complex space is the so-called instanton method in which tunneling penetration is evaluated by a classical path moving along the imaginary time [6]. A natural extension to higher-dimensional systems would be possible to a certain extent as long as the system is completely integrable [7, 8]. Complexified tori can bridge classically disconnected regions and a semiclassical argument can be developed on them. However, entirely different situations emerge even when one performs analogous extension to the system slightly perturbed from intergrable systems. This is because complexified tori are destroyed no matter how small the strength of perturbation is and the *natural boundary* may appear in complex plane.

2 Time-domain Semiclassical Analysis

First, we briefly sketch how one can describe quantum tunneling using the semiclassical technique.

Dynamical Tunnelng

The system we are concerned with is the area-preserving map:

$$F:\begin{pmatrix} p \\ q \end{pmatrix} \mapsto \begin{pmatrix} H'(p)-V'(q) \\ q+H'(p)-V'(q) \end{pmatrix}. \tag{1}$$

Qualitative feature of phase space (q,p) is controlled by the choice of kinetic term $H(p)$ and also the potential term $V(q)$.

In generic cases, phase space is composed of quatiperiodic regions ($\mathcal{Q}$) and chaotic regions ($\mathcal{C}$), and these are invariant objects in themselves and disconnected by any classical orbits. However, in quantum mechanics, the tunneling effect allows the transition between two any disconnected components of $\mathcal{Q}$ and $\mathcal{C}$, and quantum tunneling over such dynamical barrierss is particularly called *dynamical tunneling* in the literature. More precise specification or definition of quantum tunneling in the present setting is provided later.

Quantum Propagator

A standard recipe to construct quantum mechanics of the area-preserving map is first to express unitary operator in the discretized Feynman path integral form. In the momentum (p-) representation, for example, the n-step quantum propagator is written as

$$K(p_0;p_n) =< p_n|U^n|p_0 >= \int \cdots \int \prod_j dq_j \prod_j dp_j \exp\Big[\frac{i}{\hbar} S(\{q_j\},\{p_j\})\Big], \tag{2}$$

where $S(\{q_j\},\{p_j\})$ denotes the discretized action along each path The classical map (1) is recovered by imposing the variational condition $\delta S(\{q_j\},\{p_j\}) = 0$.

Semiclassical Approximation

In order to include the complex orbits that are inevitable to describe classically forbidden processes, instead of applying the stationary phase method, we evaluate the quantum propagator $< p_n|\hat{U}^n|p_0 >$ by the saddle point method. The final expression for the *semiclassical propagator* in p-representation takes the form as

$$K^{sc}(p_0;p_n) = \sum_\gamma A_\gamma(p_0,p_n) \exp\left\{\frac{i}{\hbar} S_\gamma(p_0,p_n)\right\}, \tag{3}$$

where the summation is taken over all classical paths γ satisfying given initial and final momenta, $p_0 = \alpha$ and $p_n = \beta$. $A_\gamma(p_0,p_n) = [2\pi\hbar(\partial p_n/\partial q_0)_{p_0}]^{-\frac{1}{2}}$ stands for the amplitude factor associated with the stability of each orbit γ, and $S_\gamma(p_0,p_n)$ is the corresponding classical action.

Initial Value Representation

The semiclassical sum (3) contains not only real classical orbits but also complex classical ones, the latters would be responsible for the tunneling process. One physical requirement is that since we take the p-representation, p_0 and p_n should be real-valued since they both are observables. This implies that a canonical conjugate variable q_0 does not have any constraint and may take not only real values but also complex ones, so itinerary from (p_0,q_0) to (p_n,q_n) may be complex. To include complex orbits, we extend the initial angle as $q_0 = \xi + i\eta$ $(\xi,\eta \in \mathbb{R})$. For given $\alpha,\beta \in \mathbb{R}$, we have a representation for semiclassically contributing complex paths as

$$\mathcal{M}_n^{\alpha,\beta} \equiv \{(p_0, q_0 = \xi + i\eta) \in \mathbb{C}^2 \mid p_0 = \alpha,\ p_n = \beta\ \}. \tag{4}$$

If there exist no classical orbits on the real phase space connecting two states $p_0 = \alpha$ and $p_n = \beta$, we should say that this process is classically forbidden, and bridged only by complex classical orbits

3 Tunneling Orbits in the Linear map

Before going to chaotic maps, we examine the linear map. The linear map is helpful to understand what classical objects represent quantum tunneling and to know what are new ingredients in chaotic maps.

Solutions

The linear map is given as

$$F : \begin{pmatrix} p' \\ q' \end{pmatrix} \mapsto \begin{pmatrix} p + K \sin q \\ q + \omega \end{pmatrix}, \tag{5}$$

where ω is a fixed rotation number. It is easy to show that (p_n, q_n) are expressed by (p_0, q_0) as

$$\begin{aligned} p_n &= p_0 + K_n \sin(q_0 + n\omega/2), \\ q_n &= q_0 + n\omega, \end{aligned}$$

where $K_n = K \sin(n\omega/2)/\sin\frac{\omega}{2}$. For a given initial condition $p_0 = \alpha \in \mathbb{R}$, in order to have $q_n \in \mathbb{R}$ the initial coordinate $q_0 = \xi + i\eta$ should satisfy

$$\xi = (k + \frac{1}{2})\pi - \frac{n\omega}{2} \ (k: \text{ integer}) \quad \text{or} \quad \eta = 0. \tag{6}$$

Tunneling Branches

Figure 1 illustrates a set of initial conditions that contribute to the semiclassical sum (3)

$$\mathcal{M}_n^{\alpha,*} = \{ q_0 = \xi + i\eta \mid p_0 = \alpha, \ -\infty < p_n < \infty \}. \tag{7}$$

Here we set $\alpha = 0$. The orbits satisfying the former condition in (6) are real orbits, and the latter are complex ones.

Note that tunneling branches appear in a pair-wise manner as shown in Fig. 1; the one giving exponentially decaying and the other exponentially blowing up contribution. The former is a correct tunneling branch and the latter is unphysical and should be removed as a result of *Stokes phenomenon*. The Stokes phenomenon is quite important in the complex WKB analysis, however, we do not discuss this issue here. (See [9] for example.)

Figure (2) is a schematic sketch demonstrating that pairs of tunneling branches emanating from the real Lagrangian manifold. Note that tunneling tails in the wave-function are reproduced by tunneling branches.

An important remark is that, in order to go into deep tunneling regions, one should take a large $\mathrm{Im}\, q_0 = \eta$. That is, the amount of imaginary part necessary to allow the tunneling transition is gained in the imaginary part of the initial condition. We can say, otherwise, that no dynamics is involved in the tunneling process of linear map and only the initial condition controls it. It is worthwhile to note that $\mathrm{Im}\, q_0 = \eta$ play an analogous role of imaginary time that is used in the so-called instanton method [6]. The instanton orbit runs in the imaginary direction in complex time domain, and the higher potential barriers one wants to go beyond, the deeper imaginary time domain one has to use.

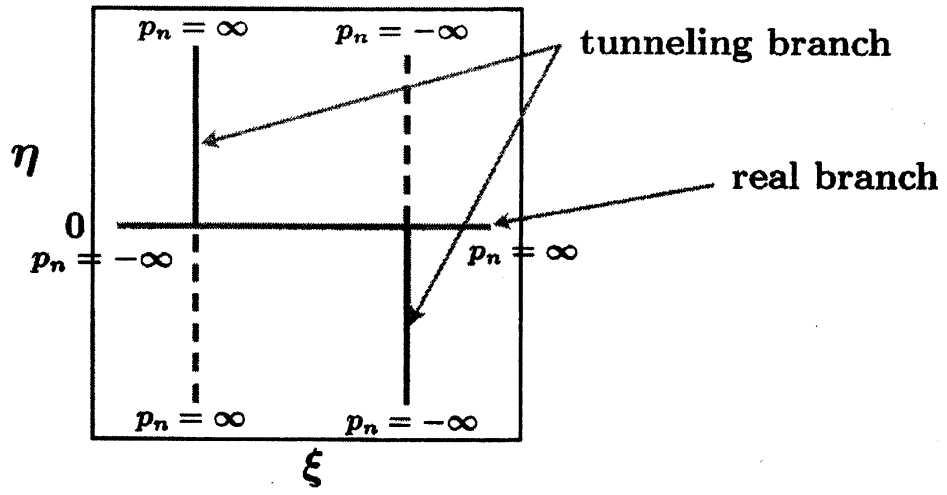

Figure 1: The initial value plane introduced as (7). The lines running in the vertical direction give the tunneling contributions.

4 Tunneling Orbits in Ideally Chaotic Maps

In contrast to the previous one, tunneling orbits in chaotic maps behave quite differently. We first see how tunneling orbits appear in the most generic situations, mixed systems.

Tunneling Orbits in The Standard Map

There are a variety of chaotic maps in the form (1) that realize mixed-type phase space. We here consider the standard map: $H(p) = p^2/2$, $V(q) = K \sin q$. Figure 3 shows a typical mixed phase space with some moderate parameter value and the corresponding initial value set $\mathcal{M}_n^{\alpha,*}$. In the semiclassical propagator, the initial state is taken as an ellipse approximating a KAM curve, not $p_0 = const$ as in the linear map. In the initial set $\mathcal{M}_n^{\alpha,*}$, two curves running in the vertical direction that exactly corresponds to the tunneling branches shown in Fig. 1. The mechanism of tunneling induced by such branches are essentially the same as the one taking place in the linear map. However, in case of the standard map, there are a huge number of branches not touching on the real axis, $\eta = 0$. All these are due to that the system is not completely integrable and the map generates chaos not only in real but also in complex plane.

We skip all the details concerning the mechanism creating tunneling tails in quantum wavefunctions [4]. Of significantly importance is that specific sequences of branches, which, as shown in Fig. 3, usually form successive chain-like structures, control the tunneling processes, meaning that we have only to focus on these specific structures. We remark that the existence of these chained objects is not limited to the standard map.

The Hénon Map

Next, we consider the Hénon map, in which both kinetic and potential terms are polyno-

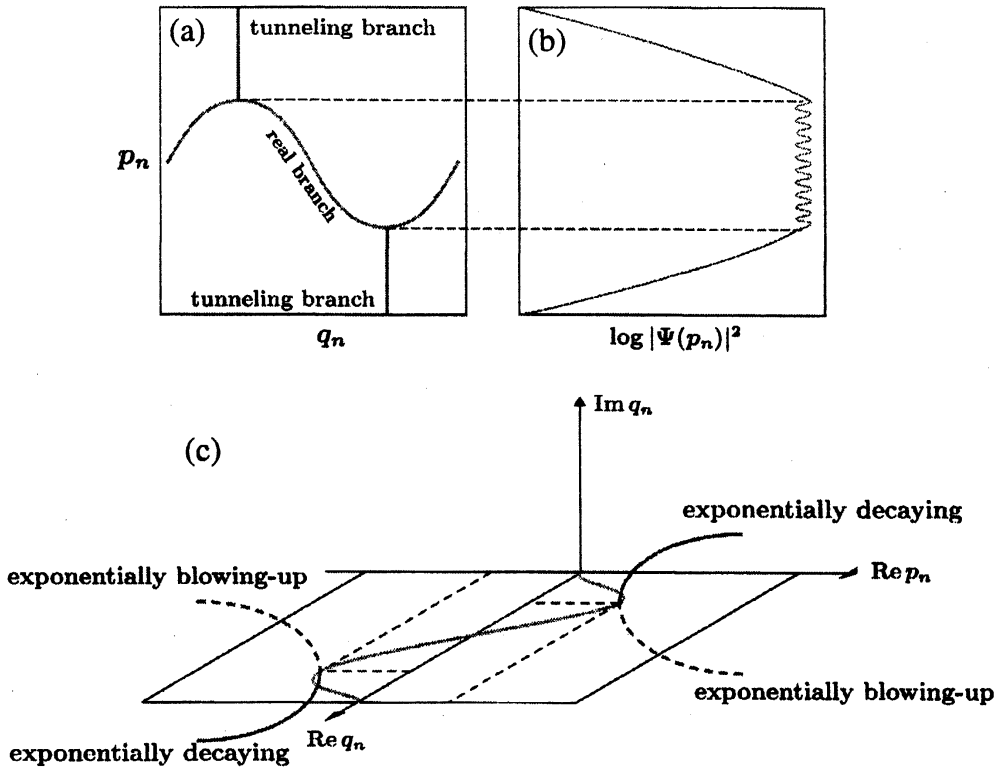

Figure 2: (a) The real Lagrangian manifold and tunneling branches. An exact form of the real Lagrangian manifold is expressed as $p_n = p_0 + K_n \sin(q_n - n\omega/2)$. (b) The wavefunction in the p- representation (schematic). (c) The real Lagrangian manifold and pairs of tunneling branches (schematic).

mial functions. There are several reasons to employ the Hénon map: the most relevant one is that complex dynamics has been and is being most extensively investigated, a part of which is introduced below. This is important because the understanding of what is going on in complex phase space is crucial.

A canonical form of the Hénon map is given as $f : (x, y) \mapsto (y, y^2 - x + a)$, but an alternative form obtained by an affine change of variables as $(p, q) = (y - x, x - 1)$ together with a parameter $c = 1 - a$ fits the present purpose:

$$F : \begin{pmatrix} q \\ p \end{pmatrix} \mapsto \begin{pmatrix} q + p \\ p - V'(q + p) \end{pmatrix}, \quad V(q) = -\frac{q^3}{3} - cq. \tag{8}$$

The Hénon map has a nonlinear paremeter a (or c) controlling the dynamics qualitatively. When $a \gg 1$, the so-called horseshoe condition is satisfied and the mapping is conjugate to the symbolic dynamics with the binary full shift [10]. All the stable and unstable manifolds intersect transversally when the horsehoe is realized and the system keeps hyperbolicity up to the first tangency point [11]. Non-wondering set forms fractal repeller on the real plane.

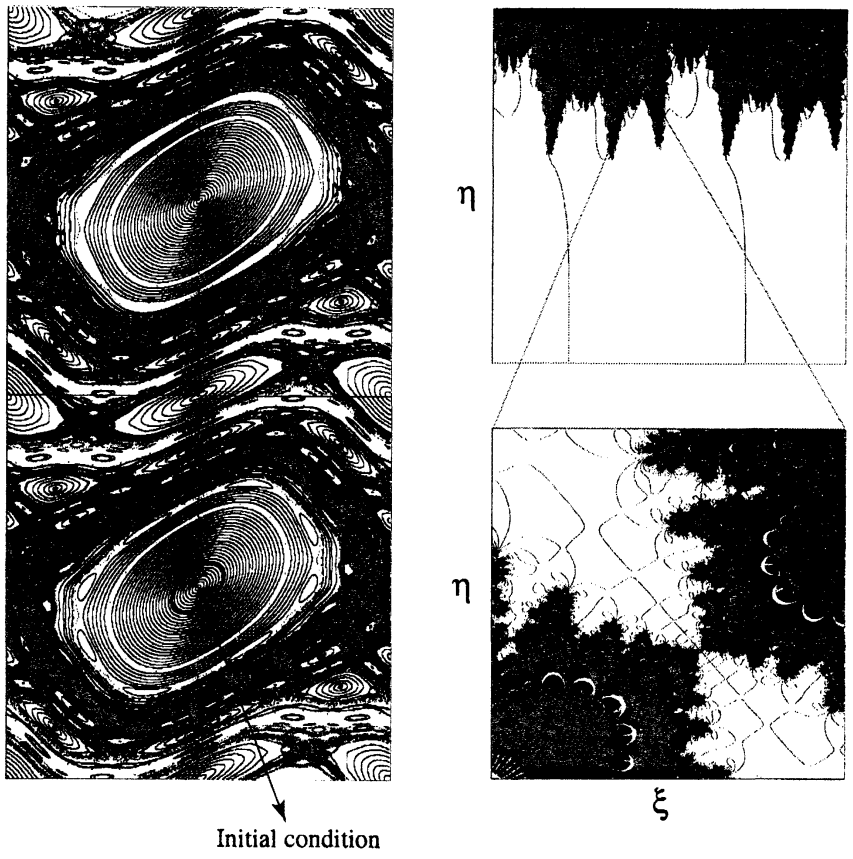

Figure 3: (a) Phase space for standard map with $K = 1.5$. An ellipse in the lower torus region is the initial condition. (b) The initial value set $\mathcal{M}_n^{\alpha,*}$ at $n = 6$ and its magnification.

The Horseshoe Limit: An Ideal Setting

The horseshoe limit provides an ideal situation where the chained structure observed in generic case appears in a genuine manner.

Figure 4 demonstrates the set $\mathcal{M}_n^{\alpha,*}$ when the parameter c is within the horseshoe locus. We notice that a similar chained structure as found in Fig. 3 is formed. A relation between $\mathcal{M}_n^{\alpha,*}$ and invariant objects in dynamical systems is read by putting the intersection of the (complex) stable manifold $W^s(p)$ of periodic orbits p with the initial value plane $\mathcal{I} = \{(q,p) \in \mathbb{C}^2 \mid p_0 = \alpha\}$. The intersection points are aligned along the chain and the labels inserted in the figure denote the binary coding for periodic orbits from where the stable manifolds $W^s(p)$ emanate. That is, for example, the dot labeled as (000) is a point at which the stable manifold of the periodic orbit whose binary coding is (000) intersects with the initial value plane $\mathcal{I}$. Recall that, in the horseshoe parameter locus, all the periodic orbits are contained in $\mathbb{R}^2$. The chained structure is associated with invariant structures in phase space in this way. As a result, the itineracy of the orbits launched on the chained structure is governed by the stable manifold attached to it. As shown in Fig. 4(b), the orbits whose initial conditions are put on the set $\mathcal{M}_n^{\alpha,*}$ approach exponentially to the real plane, reflecting that the

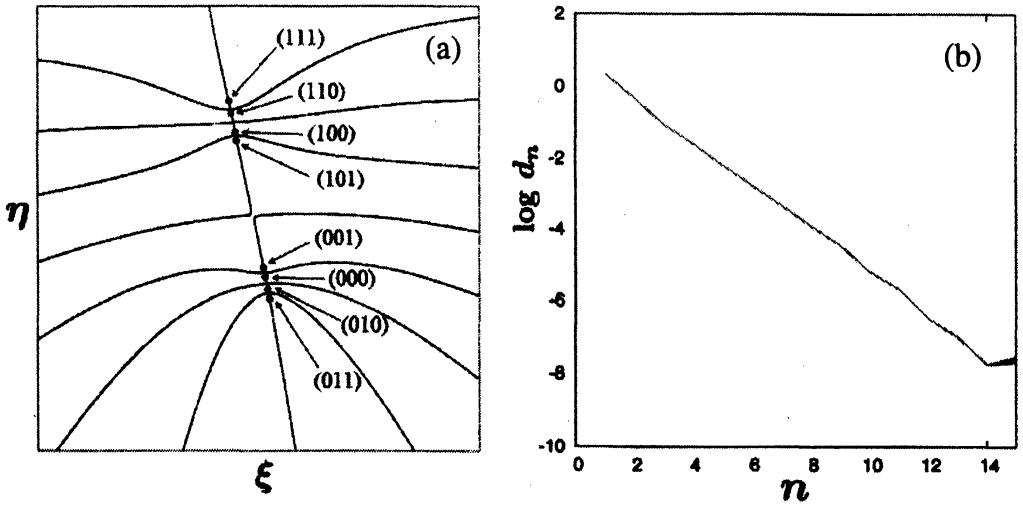

Figure 4: (a) The initial value set $\mathcal{M}_n^{\alpha,*}$ at $n = 3$ for the Hénon map in the horseshoe parameter locus. The dots represent the primary intersection points (see the definition in the text) of (complex) stable manifolds and the initial value plane $\mathcal{I}$. (b) The distance from the real plane as a function of the time step n. The orbits are launched from the points on $\mathcal{M}_n^{\alpha,*}$ and close to the intersection points.

orbits closely follow the orbits on the stable manifolds. Otherwise stated, the tunneling orbits forming chained structures are guided by the stable manifolds of the periodic orbits [12]. In a similar manner, on the chained structure found in generic mixed case (Fig. 3), the orbits starting from it also approaches the real plane exponentially. Other orbits, not forming the chain, do not shows such behavior and are not attracted from the real plane.

Tree Structure in Hyperbolic Case

It is instructive to see the situation where the system is hyperbolic but not in the horseshoe locus. Such a situation may not be so common. For instance, in the standard map, except for the so-called anti-integrable limit, phase space is composed of quasiperiodic and chaotic components. In the Hénon map, there indeed exist parameter loci in which the dynamics on the real plane is hyperbolic but cannot be reduced to the binary full shift as the horseshoe limit does so. The existence of such parameter loci was suggested in [14], and recently shown rigorously via computer-assisted proof [15].

The reason why hyperbolic but not horseshoe cases are so important in our issue is that it can be a model to examine how tunneling orbits behave when the non-wondering set is no more confined on the real plane, and thereby real and complex saddles coexist.

In the horseshoe locus, as depicted in Fig. 4, each chain runs only in the vertial direction. However, as seen in Fig. 5, the *tree structure* begins to develop in $\mathcal{M}_n^{\alpha,*}$. Furthermore, though not shown here, as the time step proceeds, we can see that the number of generation increases. Here we use the term *generation* as a rank in the hierarchical tree structures. The chained branch running in the perpendicular direction

is the first generation and horizontal one the second generation and so on.

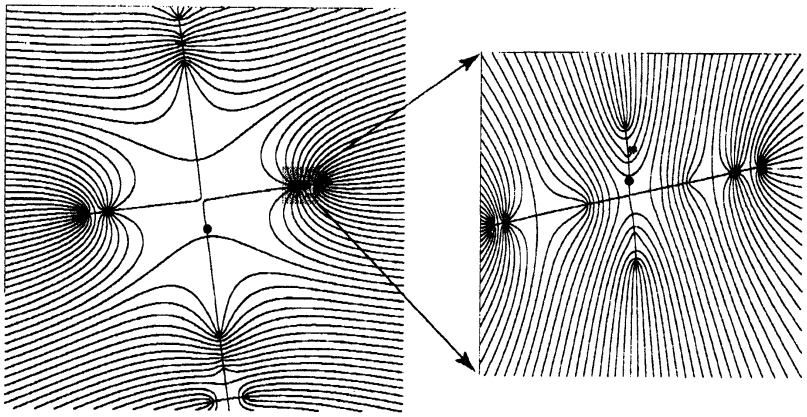

Figure 5: (a) The initial value set $\mathcal{M}_n^{\alpha,*}$ at $n = 20$ for the Hénon map in the parameter locus at which the map is hyperbolic but not has the horseshoe structure. The dots shown are some of primary intersection points of (complex) stable manifolds and the initial value plane $\mathcal{I}$. The right hand figure is a magnification of the left one.

Primary Intersection Points

To explain the implication of the tree structure, we introduce the ordering for intersection points of stable manifolds and the initial value plane $\mathcal{I}$.

Here, the *primary intersection* is defined as an intersection point at which the stable manifold $W^s(p)$ emanating from a saddle p (period n) first intersects with $\mathcal{I}$. More precisely, we specify the ordering of the intersection as follows: it is known that there is a conjugation map Φ from $\mathbb{C}$ to $W^s(p)$ such that

$$\Phi^{-1} F^n \Phi = F_{sn} \quad \text{where} \quad F_{sn}(\zeta) = \lambda^{-1}\zeta \tag{9}$$

for $\zeta \in \mathbb{C}$. Here λ denotes the maximal eigenvalue of the tangent map of F^n at p. The coordinate ζ is normalized in the sense that the map F^n is expressed by a linear transformation. Putting an appropriate domain, say $\mathcal{D}$ on the ζ-plane, containing p as the origin of ζ-plane and $\mathcal{D}' = \mathcal{D} - F_{sn}(\mathcal{D})$, the ζ plane is decomposed into a family of disjoint domains $\mathcal{D}_m = F_{sn}^{-m}(\mathcal{D}')$ $(m \in \mathbf{Z})$. Here, the primary intersection is defined as an intersection point between $\mathcal{I}$ and $W^s(p)$ in $\mathcal{D}_m$ with the minimal m in the ζ coordinate.

The dots shown in Fig. 5 are some of primary intersection points so defined. As in the horseshoe case, each intersection point is attached to a curve of $\mathcal{M}_n^{\alpha,*}$. In contrast to the horseshoe case, however, the orbits launched at points on the tree-shaped $\mathcal{M}_n^{\alpha,*}$ do not approach the real plane monotonically. To see the difference, we observe the behavior of the orbits whose initial conditions are close to the primary intersection points. We plot in Fig. 6(a) the distance from the real plane as a function of time step n and the corresponding schematic representation of the set $\mathcal{M}_n^{\alpha,*}$ is given as Fig. 6(b).

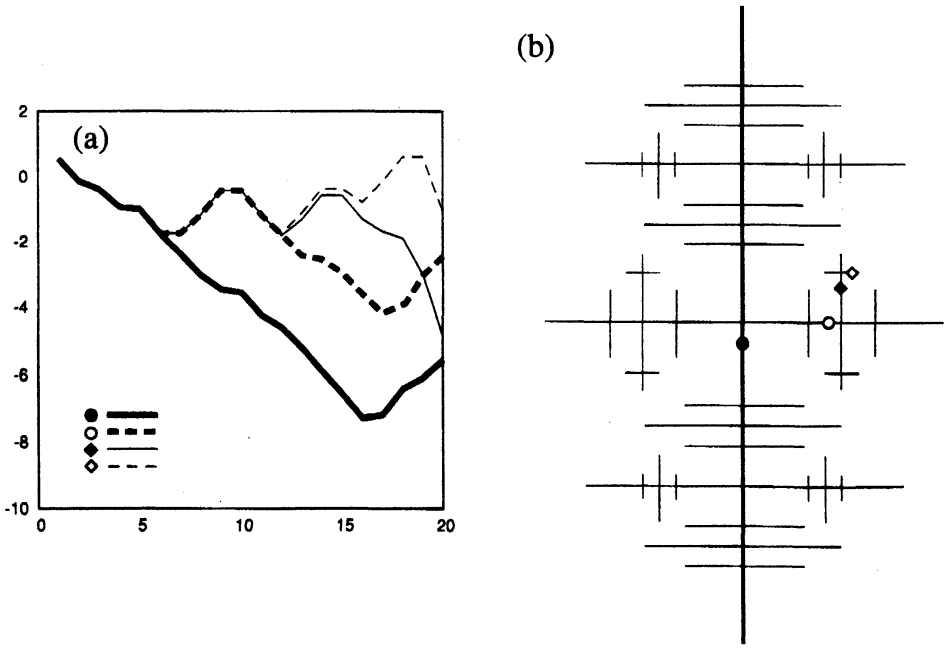

Figure 6: (a) The distance from the real plane as a function of time step n. The orbits are launched from the points on $\mathcal{M}_n^{\alpha,*}$ and close to the primary intersection points in the tree structure. (b) Tree structure and the primary intersection points (schematic).

Itineracy in The Complex Phase Space

For the interpretation of the origin of the behavior observed in Fig. 6(a), the following theorem is crucial:

Theorem[Bedford-Smillie] *For any saddle* p, $\overline{W^s(p)} = J^+$ *and also* $\overline{W^u(p)} = J^-$.

Here $J^\pm = \partial K^\pm$ and $K^\pm = \{ (p,q) \mid \|F^n(p,q)\|$ is bounded $(n \to \pm\infty) \}$. Since $K^\pm = J^\pm$ in the hyperbolic case, the above theorem claims that any stable manifold is dense in the forward bounded orbits K^+.

Now, let $\mathbf{r}_i$ and $\mathbf{c}_j$ be the saddles in the real and complex plane, respctively. We then introduce the primary intersections between $\mathcal{I}$ and W^s of these two kinds of saddles, say $\mathbf{r}_1$ and $\mathbf{c}_1$; they are denoted by $\mathbf{X}_1 (\in W^s(\mathbf{r}_1) \cap \mathcal{I})$ and $\mathbf{Y}_1 (\in W^s(\mathbf{c}_1) \cap \mathcal{I})$, respectively (see Fig. 7).

Consider a side branch in the second genetation, which is attached to the intersection point denoted by $\mathbf{Y}_1 = W^s(\mathbf{c}_1) \cap \mathcal{I}$. Since $\mathbf{Y}_1$ is located close to $\mathbf{X}_1$, the trajectories starting at $\mathbf{X}_1$ and $\mathbf{Y}_1$ trace similar itinerary in the very initial time stage. But the orbit launched at the $\mathbf{Y}_1$ finally approaches $\mathbf{c}_1$ by definition and cannot reach the real phase space. However, the fact $\overline{W^s(p)} = J^+$ implies that in a very close neighborhood of $\mathbf{Y}_1$ there exists an intersection $\mathbf{X}_2' \in W^s(\mathbf{r}_2) \cap \mathcal{I}$ of a real saddle $\mathbf{r}_2$ ($\mathbf{r}_2$ can be $\mathbf{r}_1$). Let the primary intersection of $W^s(\mathbf{r}_2)$ and $\mathcal{I}$ be $\mathbf{X}_2$, then the trajectory from $\mathbf{X}_2$ converges directly to $\mathbf{r}_2$, whereas the trajectory from $\mathbf{X}_2'$ first approaches $\mathbf{c}_1$ because $\mathbf{X}_2'$ is very close to $\mathbf{Y}_1 = W^s(\mathbf{c}_1) \cap \mathcal{I}$ and next converge to $\mathbf{r}_2$, which means that $\mathbf{X}_2'$ is the secondary intersection of $W^s(\mathbf{r}_2)$ with $\mathcal{I}$. In other words, the trajectory from $\mathbf{X}_2'$ makes a side trip in the complex domain before accessing to the real plane.

In the same way, there should exist $\mathbf{Y}_2' = W^s(\mathbf{c}_2) \cap \mathcal{I}$ which is located just at the

side of $\mathbf{X}_2'$, where $\mathbf{c}_2$ denotes another complex saddle. The side chain of the third order is realized very close to the tirtiary intersection $\mathbf{X}_3''$ of the intersction $\mathcal{I} \cap W^s(\mathbf{r}_3)$, if n is taken large enough. Inductively, the m-th order generation, germinates from the $(m-1)$-th order generation.

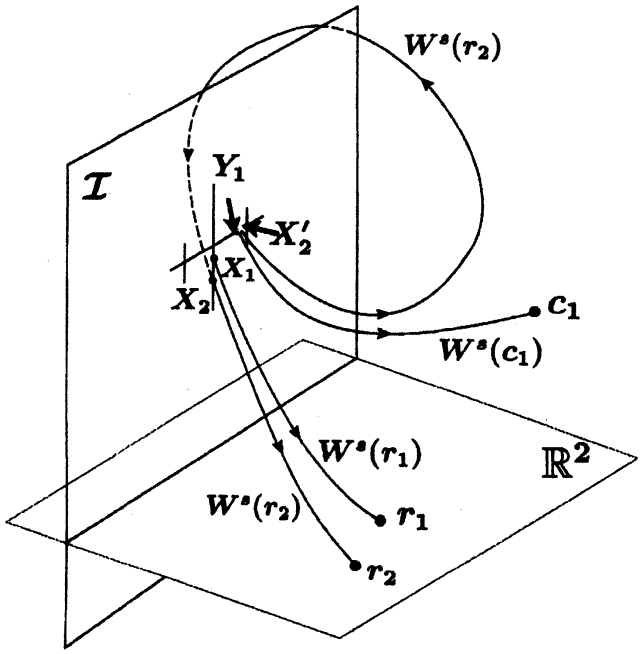

Figure 7: Initial value plane $\mathcal{I}$ and stable manifolds for real saddles (schematic).

As predicted by the theorem $\overline{W^s(p)} = J^+$ and numerical observations imply that there exist a rich variety of tunneling paths wandering over complex phase space before reaching close to the real plane. Ishii gave a rigorous statement supporting such an aspect [12]. It assures the existence of orbits that allow trajectories exhibiting chaotic itinerancy over the complex saddles:

Theorem[Ishii] *Let* $0 < h_{\mathrm{top}}(F|_{\mathbb{R}^2}) < \log 2$ *and let* p_i $(1 \leq i \leq N)$ *be saddle periodic points in* $\mathbb{C}^2 \setminus \mathbb{R}^2$. *Take any positive integers* k_i *and any neighborhood* U_i *of* p_i $(1 \leq i \leq N)$. *Then, there exists a point* $z \in \mathbb{C}^2 \setminus \mathbb{R}^2$ *such that its orbit stays in* U_i *at least* k_i*-times iterates and* $\lim_{n\to\infty} d(F^n(z), \mathbb{R}^2) = 0$.

The convergent theorem of currents is a central result of Bedford and Smillie and many results follow from it [17, 16, 18]. The above theorem essentially uses the results of [18]. An important fact is, as mentioned below, that the convergent theorem applies not only to hyperbolic but also to any cases including mixed phase space. Therefore, it is natural to expect that the behavior just sketched above is not limited to the hyperbolic case. In fact, the orbits launched at a chained branch in the higher generation, for example as given in Fig. 3, exhibit essentially in the same behavior.

Why Are Chained Structures So Important?

Up to now, we only saw the behavior of complex orbits that contribute to the semiclassical propagator (3). The readers may have questions as to why the chained structures found commonly in the initial value plane is so important in our tunneling problem. We have entirely skipped this topic.

The main reason is that, as shown in Fig. 4, the orbits forming the chain structure approach the real plane exponentially. Correspondingly, the imaginary part of action, $\mathrm{Im}\, S_n$, converges rapidly and we may expect that $|\mathrm{Im}\, S_n|$ takes the smallest values as compared with those for the orbits taking side trip, unless some nontrivial cancellation mechanism works in itinerating orbits. Since the weight of each term in the semiclassical sum (3) is almost controlled by $\mathrm{Im}\, S_n$, the orbits that gain the minimal $\mathrm{Im}\, S_n$ are most dominant contributors in the sum. This is a rough reasoning for the importance of the chained objects. It is not yet clear that the orbits wondering in complex space, as found in Fig. 6(a), play some roles in the tunneling problem. If they make non-negligible contributions, we may say that *genuine complex chaos* appears in quantum tunneling. More detailed aruguemts of *observability* of complex chaos in quantum tunneling will be discussed in [13].

5 Tunneling Orbits in Mixed Phase Space

Initial and Final Manifolds in Semiclassical Dynamics

As often emhpasized, the most natural and important situation is that KAM curves and chaotic regions coexist in phase space. That is, the transition from KAM regions to chaotic seas has particularly to be investigated. To focus our problem more sharply, we again make clear the setting of the semiclassical argument.

So far, we have taken p-representation like eq. (2). However, we can freely replace it to other representations. For example, we may take the coherent representation $K(q_n, p_n; q_0, p_0) = < q_n, p_n|\hat{U}^n|q_0, p_0 >$. Here $|q, p >= |a >$ denotes the coherent state with $a = (q + ip)/\sqrt{2}$. We have a similar semiclassical expression as

$$K^{sc}(q_n, p_n; q_0, p_0) = \sum_{\gamma} A_\gamma(p_0, q_0) \exp\left\{\frac{i}{\hbar} S_\gamma(p_0, q_0)\right\}, \tag{10}$$

where the sum is taken over all classical paths satisfying given initial and final coherent states, *i.e.*, $q_0 + ip_0 = q_\alpha + ip_\alpha$, $q_n - ip_n = q_\beta + ip_\beta$. Note that the variables $q_\alpha, p_\alpha, q_\beta, p_\beta$ take real values whereas q_0, p_0, q_0, p_0 can take complex ones [19, 20]. Introducing the variables $Q = q + ip$ and $P = q - ip$ where $q, p \in \mathbb{C}$, semiclassically contributing complex paths are given as

$$\mathcal{M}_n^{\alpha,\beta} \equiv \{(Q_0, P_0) \in \mathbb{C}^2 \mid Q_0 = \alpha,\ P_n = \beta,\ \ \alpha = q_\alpha + ip_\alpha,\ \beta = q_\beta - ip_\beta,\ \}. \tag{11}$$

Note that in any representation the manifold of initial or final states is one-dimensional complex manifold, thereby the space of the search parameter forms one-dimensional complex plane. This is interpreted as a manifestation of uncertainty principle of quantum mechanics.

Convergent Theorem and Mixing Property in Complex Phase Space

The *semiclassical dynamics* is therefore just to follow the time evolution of a one-dimensional complex manifold with a boundary condition imposed on the final state. The final state is also expressed as one-dimensional complex manifold. We again recall that the asymptotic behavior of wide classes of manifolds is well controlled using potentially theoretic arguments of complex dynamical systems [17, 16, 18], More precisely, the following *convergent theorem of currents* tells us how one-dimensional manifold behaves asymptotically:

Theorem[Bedford-Smillie]
For a complex one-dimensional locally closed sub-manifold M in either $J^{\pm}$ or an algebraic variety, there is a constant $\gamma > 0$ so that

$$\lim_{n\to+\infty} \frac{1}{2^n}[F^{\mp n}M] = \gamma \cdot dd^c G^{\pm}(x,y) \tag{12}$$

in the sense of current, where $[M]$ is the current of integration of M, i.e. $[M](\phi) \equiv \int_M \phi|_M$. *In this statement, $G^{\pm}(x,y)$ represents the Green function given by*

$$G^{\pm}(x,y) \equiv \lim_{n\to\pm\infty} \frac{1}{2^n} \log^+ \|F^n(x,y)\|\,, \tag{13}$$

where dd^c is the complex Laplacian,

$$dd^c u \equiv 2i \sum_{j,k} \frac{\partial u}{\partial z_j \partial \bar{z}_k} dz_j \wedge d\bar{z}_k \tag{14}$$

The statement claims that an arbitrary algebraic curve in $\mathbb{C}^2$, for example our initial manifold given as $p_0 = \alpha \in \mathbb{R}$, converges to the support of $dd^c G^{\pm}(x,y)$. Moreover,

Theorem[Bedford-Smillie] *μ is mixing and the hyperbolic measure.*

Here $\mu \equiv \mu^+ \wedge \mu^-$ and $\mu^{\pm}$ is induced by the Green function as

$$\mu^{\pm} \equiv \frac{1}{2\pi} dd^c G^{\pm}(x,y). \tag{15}$$

The complex equilibrium measure μ thus defined becomes a unique maximal entropy probability measure [17, 16, 21, 18].

Implications in The Tunneling Problem

Since the asymptotic behavior is so described by the convergent theorem, we obtain theorems on the relation between tunneling orbits and the Julia set in the forward direction by taking into account the final states also [12]. The result indeed supports and is consistent with numerical observations illustrated in Figs. 3, 4, and 6. In this sense, we can say that, in contrast to tunneling orbits in the linear map, the complex orbits behind tunneling processes in chaotic systems have truly different characters.

As stressed in section 3, tunneling penetration does not occur as a result of dynamics in the linear map, but gaining the imaginary part of the initial condition makes it possible. On the hand hand, in the Hénon map, due to the mixing property stated above, arbitrary neighborhoods of the points in the Julia set are connected by the dynamics in complex plane. To see more explicitly how the mixing property plays

the role, the coherent state representation is useful since the coherent state is a minimal wavepacket, and is an object closes to an orbit in classical dynamics. For any neighborhood U_α, U_β of initial and final points, (q_α, p_α) and (q_β, p_β) in the coherent representation, there exist a time step N such that $f^N(U_\alpha) \cap U_\beta \neq \emptyset$. Since the neighborhood U_α should be taken as an open set in $\mathbb{C}^2$, the orbit connecting between U_α and U_β may not be contained in the initial manifold $\mathcal{M}_n^{\alpha,\beta}$. However, we can find another initial state (q'_α, p'_α) that can be taken arbitrarily close to the original point (q_α, p_α) which contains a desired orbit. In other words, although one cannot say that a set $\mathcal{M}_n^{\alpha,\beta}$ always contains a connecting orbit, there is a wavepacket arbitrarily close to the original one whose initial plane $\mathcal{M}_n^{\alpha',\beta'}$ contains such a connecting orbit. The tunneling transition, reflecting the mixing property of the complex measure μ, takes place in this way.

Complexified KAM Curves and Natural Boundaries

As mentioned, theorems of Bedford and Smillie are suggestive and certainly give a fundamental principle for the semiclassical description of quantum tunneling processes. However, only to know the existence of invariant measure having such nice properties is not enough to get further predictive view in tunneling phenomena. since the most important process, that is, the transition from the region dominated by KAM curves to chaotic regions, necessarily involves many delicate issues in the problem of nearly integrable Hamiltonian dynamics, so more precise information on complex structures in such regions is strongly required.

In particular, we need to discuss the role of *complexified KAM curves*. To this end, the works done by several authors who studied the domain of analyticity of complexified KAM curves become significant clues [22, 23]. The aim in those works was to specify a critical value of the perturbation parameter K_c at which the last KAM circle disappears, and also to study the universality of the critical function $K(\omega)$: the breakdown threshold of the KAM curve with rotation number ω. Here we will see that this subject is indeed of fundamental importance in the tunneling problem.

A standard recipe to consider the analyticity domain of KAM curves is first to express KAM curves parametrically as

$$C_\omega : \begin{pmatrix} p \\ q \end{pmatrix} = \begin{pmatrix} 2\pi\omega + u(\varphi,\omega) - u(\varphi - 2\pi\omega, \omega) \\ \varphi + u(\varphi,\omega) \end{pmatrix}, \tag{16}$$

where $u(\varphi,\omega)$ is determined by the following functional equation:

$$u(\varphi + 2\pi\omega, \omega) - 2u(\varphi,\omega) + u(\varphi - 2\pi\omega,\omega) = V'(\varphi + u(\varphi,\omega)). \tag{17}$$

The dynamics on the curve C_ω is given in the φ-variable as a constant rotation $\varphi_{n+1} = \varphi_n + 2\pi\omega$. For a given rotation number ω, the existence of an analytic KAM curve is equivalent to the existence of a positive radius of convergency of the Lindstedt series,

$$u(\varphi,\omega) \equiv \sum_{k=1}^{\infty} K^k \sum_{\nu \leq k} e^{i\nu\varphi} u_\nu^{(k)}(\omega). \tag{18}$$

As first suggested in Ref. [22], making analytical continuation of the Lindstedt series to the complex plane, one can do it at most to a certain domain of φ-plane and there possibly exist a natural boundary. The existence of the natural boundary implies that

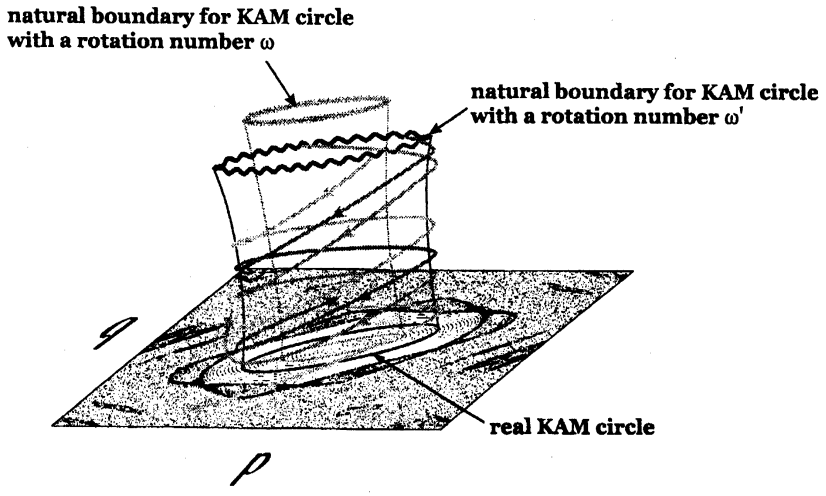

Figure 8: Natural boundaries of KAM circles (schematic). The complex orbits which describe tunneling processes are also inserted in the figure. Those orbits launched almost around natural boundaries and go down to the real plane. The distance from the real plane decreases exponentially, just as shown in Fig. 4(b) and the bold line of Fig. 6(a).

KAM circles cannot be globally invariant in complex plane. Numerical observations suggest the shape of the boundary is fractal in (q,p)-plane. We schematically draw an aspect in Fig. 8.

Mixing in the Complexified KAM Regions ?

The orbits on KAM curves are bounded both in the forward and backward directions, so they are contained in the filled-in Julia set $K = K^+ \cap K^-$. Note that numerical tests suggest that $K^\pm$ have no interior points [9]. There is no rigorous proof validating those numerical results, but if $K^\pm$ have no interior points, $J = K$ follows.

Next we ask the relation between J and $J^* = \mathrm{supp}\,\mu$. In case the system is hyperbolic, $J = J^*$ holds, but in general it was at most proved that $J^* \subset J$. In non-hyperbolic or mixed systems, both possibilities remain: (i) $J = J^*$ or (ii) $J \neq J^*$. If the former holds, it immediately follows that $\{\text{KAM curves}\} \subset J^*$. Since the mixing property holds on J^*, a more specified situation just mentioned above is realized, that is the mixing property of complex dynamics allows the connection between two separated regions via the real dynamics. On the other hand, if the case (ii) is true, it can happen that such orbits do not necessarily exist.

It is not an easy task to check which situation is really the case even numerically. What we have presented in Fig. 9 is a typical behavior of the orbits sandwiched between complexified KAM curves. Here we put an initial point (q_0, p_0) such that $(\mathrm{Re}\,q_0, \mathrm{Re}\,p_0)$ is on a certain KAM circle and $|\mathrm{Im}\,q_0|, |\mathrm{Im}\,p_0| \ll 1$. The orbit so located very close to the real plane initially rotate along a KAM curve that is closest to the initial point but it gradually leaves the real plane. Then it moves in complex phase space in a spiral way. In almost all cases, however, the orbits moving up in such a way diverge to infinity finally. More precisely, until a certain finite boundary, orbits rotate along the wall of

complexified KAM curves as shown in Fig. 8, but once they reach the boundary, they quickly fly away to infinity. The fact that typical orbits behave in this way is entirely consistent with the fact that $K^{\pm}$ has no interior points because arbitrary chosen initial points in complex plane should belong to $\mathbb{C}^2 \backslash K$.

On the other hand, if the initial point is chosen very carefully, we can find the orbits such that they initially leave the real plane and tend to boundaries in a similar way as above, but they again go back to and approaches the real plane. Figure 9 exactly demonstrates such an example. An important fact is that, as shown in Fig. 9(b), once the orbit goes back close to the real plane, it rotates along the KAM curve that is different from the initially located one. Several different circles observed in Fig. 9(b) is projections of an orbit belonging to different time intervals. This numerical experiment strongly implies that KAM curves on the real domain are indeed bridged via complex orbits in the Julia set.

We should note, however, that this result does not necessarily suggest $J = J^*$. If $J = J^*$, due to the result of Bedford and Smillie again, there must exist saddle periodic points in any close neighborhood of complexified KAM circles, which is just the wall surface of cylinders shown in Fig. 8. Such an aspect cannot not be so easily verified even numerically.

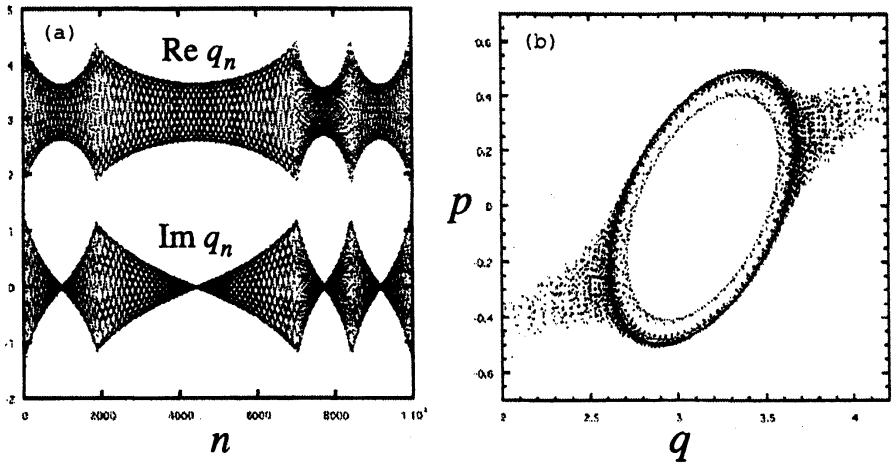

Figure 9: (a) Temporal behavior of an orbit that is put close to the real plane. $(\mathrm{Re}\, q_0, \mathrm{Re}\, p_0)$ is on a KAM curve on the real plane. In the temporal behavior, when $\mathrm{Im}\, q_n$ is almost zero, $\mathrm{Im}\, p_n$ takes also almost zero. Thus, the orbit is very close to the real plane each time focusing of $\mathrm{Im}\, q_n$ occurs. (b) Projection of an orbit on to (q_n, p_n) plane.

Natural Boundaries of KAM Curves and The Julia Set

As mentioned, a semiclassical state is identified as a one-dimensional complex manifold. For the moment, we forget restrictions originating from quantum mechanics and concentrate only on the semiclassical dynamics, that is, the dynamics of one-dimensional complex manifolds.

Suppose, as a *Gendanken Experiment*, an initial semiclassical manifold put exactly on a certain KAM curve with a rotation number ω. The complexification is made by

extending the angle variable φ in the Lindstedt series (18) to the complex plane as $\varphi = \varphi' + i\varphi''$. The initial value plane thus complexified is nothing but an analytical extension of the KAM curve with a given rotation number ω. Since KAM curves with different rotation numbers give different invariant sets, the transition between them is still forbidden so long as the Fourier expansion (18) provides a complex analytic function. However, natural boundaries possibly appear, thereby we cannot extend the initial value plane beyond them. The best possible way to make the orbits be confined within a KAM curve would be the procedure described here.

On the other hand, the convergent theorem applies at least to complex algebraic curves. If we take a complex algebraic curve as an initial semiclassical set, forward iteration of it, roughly speaking, tends to J^- and the backward to J^+. Therefore, such classes of complex one-dimensional curves are not confined in KAM curves and necessarily spread over chaotic seas.

If not only algebraic curves but also *any* semiclassical states cannot stay within KAM curves, we may say that the transition between (real) classically forbidden regions takes place in the purely classical dynamics. To make the situation more transparent, we have to clarify the relation between natural boundaries of KAM curves and the Julia set. This would become a core question.

Estimating the imaginary action $\mathrm{Im}\, S_n$ is the most relevant task in the semiclassical analysis of quantum tunneling. Numerical experiments, together with an analysis for the linear model discussed in section 3, suggest that this is roughly proportional to the length of integrable branches in the initial value plane $\mathcal{M}_n^{\alpha,*}$. More precisely, as shown in Fig. 3 two integrable branches emanating from the real branch $\eta = 0$ extends in the imaginary direction and they disappear in the aggregated region in which chained structure are hidden. The length of integrable branches is then almost equal to the imaginary part of the lower boundary of those aggregated branches. It was also found numerically that natural boundaries of complexified KAM curves are almost located along the lower boundary of aggregated branches [13]. Therefore, $\mathrm{Im}\, S_n$ must be closely connected with the width of the analyticity domain of KAM curves, that is, the radius of convergence of Lindstadt series must control the tunneling action. If this is indeed the case, it can happen that the tunneling probability varies irregularly as a function of the rotation number ω since the radius changes in a fractal manner. So, it would become extremely important for the quantum tunneling problem to study how the nature of natural boundaries affect the tunneling action $\mathrm{Im}\, S_n$.

The present note is written on the basis of the collaboration with Y. Ishii and K.S. Ikeda. The author thanks E. Bedford for his stimulating suggestions.

References

[1] S. C. Creagh, in *Tunneling in complex systems* ed. by S. Tomsovic (World Scientific, Singapore, 1998) pp. 35 - 100.

[2] O. Bohigas, S. Tomsovic and D. Ullmo Phys. Rep. **223**, 43-133 (1993); S. Tomsovic and D. Ullmo Phys. Rev E **50**, 145-162 (1994).

[3] S.D. Frischat and E. Doron, Phys. Rev. E**57**, 1421-1443 (1999).

[4] A. Shudo and K. S. Ikeda, Phys. Rev. Lett. **74**, 682-685 (1995); Physica D**115**, 234-292 (1998); T. Onishi, A. Shudo, K. S. Ikeda and K. Takahashi, Phys. Rev. E **68**, 056211-1-22 (2003).

[5] K. Takahashi and K.S. Ikeda, Ann. Phys. (NY) **284**, 94 - 140 (2000); J. Phys. A **36** (2003) 7953; EuroPhys. Lett. **71**, 193 - 199 (2005).

[6] J.S. Langer, Ann. Phys. **54**, 258-275 (1969); S. Coleman, in *The Whys of Nuclear Physics*, A.Zichin(ed.) (Academic, N.Y., 1977); W.H. Miller, J. Chem. Phys. **53**, 1949-1959 (1970); Adv. Chem. Phys. **25**, 69-177 (1974).

[7] M. Wilkinson, Physica D **21**. 341-354 (1986); M. Wilkinson and J. H. Hannay, Physica D **27**, 201-212 (1987).

[8] S. C. Creagh, J. Phys. A **27**, 4969-4993 (1994).

[9] A. Shudo, RIMS Kôkyûroku, **1424** 184-199 (2005).

[10] R. Devaney and Z.Nitechi, Commun. Math. Phys., **67**, 137-146 (1979).

[11] E. Bedford and J. Smillie, Ann. Math., **160**, 1-26 (2004).

[12] A. Shudo, Y. Ishii and K.S. Ikeda, J. Phys. A **35**, L225-L231 (2002). A. Shudo, Y. Ishii and K.S. Ikeda, to be submitted.

[13] A. Shudo, Y. Ishii and K.S. Ikeda, to be submitted.

[14] M.J. Davis, R. S. MacKay,and A. Sannami, Physica D **52** 171-178 (1991).

[15] Z. Arai, *On hyperbolic plateaus of the Héon maps*, preprint (2005).

[16] E. Bedford, and J. Smillie, J. Amer. Math. Soc. **4**, 657-679 (1991).

[17] E. Bedford, and J. Smillie, Invent. Math. **103**, 69-99 (1991).

[18] E. Bedford, M. Lyubich and J. Smillie, Invent. Math. **112**, 77-125 (1993).

[19] J.R. Klauder, In *Path Integrals,* edited by G.J. Papadopoulos and J.T. Devreese, NATO Advanced Summer Institute (Plenum, New York, 1978), p. 5; J.R. Klauder, in *Random Media,* edited by G. Papanicolauou (Springer-Verlag, New York, 1987) p. 163.

[20] S. Adachi, Ann. Phys. **195**, 45- (1989).

[21] J. Smillie, Ergod. Th. and Dynam. Sys. **10**, 823- 827 (1990).

[22] J.M. Greene and I.C. Percival, Physica D **3**, 530-548 (1981); I.C. Percival, Physica D **6**, 67-77 (1982).

[23] S. Marmi, J. Phys. A **23**, 3447-3474 (1990); A. Berretti, and L. Chierchia, Nonlinearity, **3**, 39-44 (1990); A. Berretti and S. Marmi, Phys. Rev. Lett. **68**, 1443-1446 (1992); A. Berretti, A. Celletti, L. Chierchia and C. Falcolini, J. Stat. Phys. **66**, 1613-1630 (1992).